ELSEVIER

Catalysis Today 79–80 (2003) 159–167

CATALYSIS TODAY

www.elsevier.com/locate/cattod

Effects of macroscopic hydrodynamics on heat transfer in a three-phase fluidized bed

Tsao-Jen Lin*, Chiu Hung-Tzu

Department of Chemical Engineering, National Chung-Cheng University, Chia-Yi 621, Taiwan, ROC

Abstract

The macroscopic hydrodynamics and heat transfer of a two-dimensional (2D) three-phase fluidized bed have been quantitatively studied using particle image analyzer (PIA) and heat transfer probe, respectively. Three flow regimes transiting with increasing gas velocity are investigated, including dispersed and coalesced bubbling regimes characterized by two flow conditions (4- and 3-region flow). These flow regimes are comprised of different macroscopic structures, which are profoundly dominate the local heat transfer distribution. Generally, the bubble stream can enhance the heat transfer due to inducing the turbulent intensity, while the vortex acts like a barrier to inhibit the heat transfer. Different solid holdups are introduced into the flow to examine the effect on the heat transfer. It is found that the solid particles can initially increase the collision frequency between the solid particles and heating object, which leads to the increase of heat transfer. However, increasing the solid holdup over 8% becomes a negative effect on the heat transfer. The average heat transfer coefficient increases with the liquid and gas velocities in the beginning, and then levels off with further increasing the liquid and gas velocities.

Keywords: Macroscopic hydrodynamics; Heat transfer; Three-phase fluidization; Particle image analyser

1. Introduction

Three-phase fluidized beds have been extensively adopted in many industrial processes, such as petrochemical, biochemical, and environmental processes [1,2]. The high heat-transfer rate is recognized as one of the main characteristics for the wide application of three-phase fluidization. The highly mixed hydrodynamic structures induced by the bubble movement and the interactions from particles and liquid, dictate the heat transfer in three-phase fluidized bed reactors. Hence, a better understanding of effects of hydrodynamic structures on heat transfer is an important task for improving the design and the operation of three-phase fluidized bed reactors.

Little data are available for the instantaneous relationship between the heat transfer and the hydrodynamics of the three-phase fluidized bed reactors, because of the complexity of the hydrodynamics structures in the beds. Most of previous studies only concern the overall average heat transfer between an immersed heating objects and flow by placing the heat transfer probe at the central region of small three-phase fluidized bed reactors [3–9]. However, the probes employed previously for measuring heat transfer were so large that the flow pattern is significantly influenced, which leads to lose the information pertaining to the time-variant local hydrodynamics.

It is well known that the heat transfer in the three-phase fluidized bed reactors has a strong dependence on the liquid phase properties, but a weak dependence on gas phase properties. General speaking, the heat transfer coefficient (h) increases with gas and liquid

* Corresponding author. Fax: +886-5-2720411x33405.
E-mail address: chmtjl@ccunix.ccu.edu.tw (T.-J. Lin).

0920-5861/03/$ – see front matter © 2003 Elsevier Science B.V. All rights reserved.
doi:10.1016/S0920-5861(03)00021-X

Nomenclature

h	local heat transfer coefficient (W/m^2 K)
h_{ave}	overall heat transfer coefficient (W/m^2 K)
u	averaged horizontal liquid velocity (cm/s)
U_G	superficial gas velocity (cm/s)
U_L	superficial liquid velocity (cm/s)
v	averaged vertical liquid velocity (cm/s)

velocities, size and density of the particles, the thermal conductivity, and the heat capacity of the liquid, but decreases with increasing liquid viscosity [10–13]. Baker et al. [3] reported that the h initially has a quit significant effect by the gas velocity to a power between 0.059 and 0.34, because of inducing the turbulent intensity as the gas flow is injected into the liquid–solid systems. The effect on the h will level off with further increasing gas velocity. On the other hand, the h increases with liquid velocity due to the generation of micro-eddies to oscillate the motion of the fluidized particles [5,14]. Further increasing liquid velocity, h reaches to a maximal value, and then gradually decreases as a result of reducing the solid particle fraction and leading to the reduction of the mixing intensity. As introducing solid particles into the reactor, the contacting frequency between the particles and the heating object is thought to be the key mechanism of the heat transfer in the three-phase systems. Hence, particle size and solid holdup play vital factors for the heat transfer through influencing the turbulent intensity and bubble dynamics [15,16]. To sum up, all the above factors can be ultimately attributed through the hydrodynamics in the three-phase systems. However, till now, no experimental evidence of the effect of the flow structure on the heat transfer has been provided.

In the three-phase fluidization, three major macroscopic hydrodynamic structures shifting with gas velocities are commonly identified, such as dispersed bubble regime, churn turbulent regime, and slugging regime [17,18]. Menzel [19] measured the point axial and radial liquid velocities and found that the radial profile of the Reynolds shear stress is corresponded well to that of the axial liquid velocity. The results are similar to those of Yang et al. [20] measured by a computer-automated radioactive particle tracking (CARPT) technique. Because of the limitation of the measuring techniques and the complicated mechanisms of the systems, no quantitative instantaneous flow information for a whole flow plane can presently be obtained through the use of traditional, both intrusive and non-intrusive, measurement techniques. Till lately, by the utilization of advanced image acquisition and the computer processing technique, particle image velocimetry (PIV) overcomes the above limitations and provides a quantitative instantaneous full flow field in two-dimensional (2D) columns [21–23]. The 2D systems have been employed to yield important quantitative flow information of three-phase fluidization [24], which is compatible to that in the three-dimensional (3D) systems [25]. In addition, Chen and Fan [26] found through the qualitative flow visualization that the flow structures in 2D and 3D three-phase fluidized beds are similar. Therefore, although there are limitations in similarity between 2D and 3D systems, the structures present in the flow field in 2D systems can qualitatively enlighten a better understanding of those in 3D systems. According to Higbie's surface renewal theory combined with Kolmogoroff's theory, the hydrodynamic characteristics are the main dominant factor for the heat transfer in three-phase fluidized beds [4]. Li and Prakash [27] reported that the liquid circulation patterns affiliate to the heat transfer rate through varying the position and orientation of the heat transfer probe in the beds. Besides, the macroscopic hydrodynamic structures are significantly different with gas velocity and solid holdup according to the previous findings [21,28]. Hence, it is worth to explore the relationship between the hydrodynamic structures and the heat transfer in 2D three-phase fluidized bed reactors.

2. Experimental

Fig. 1 gives the schematic diagram of test facility. The main body of the 2D acrylic column is 50 cm in width, 1.2 cm in depth, and 220 cm in height. Below the viewing section is the gas distributor, which consists of 0.16 cm-ID tube injectors, flush and horizontally mounted on the column wall. There are total nine injectors arranged in the radial direction with the interval of 5 cm apart. The gas flow through each injector is individually regulated by a needle valve connected to the plenum compartment outside of the bed. Air is used as gas phase. Glass beads of mean

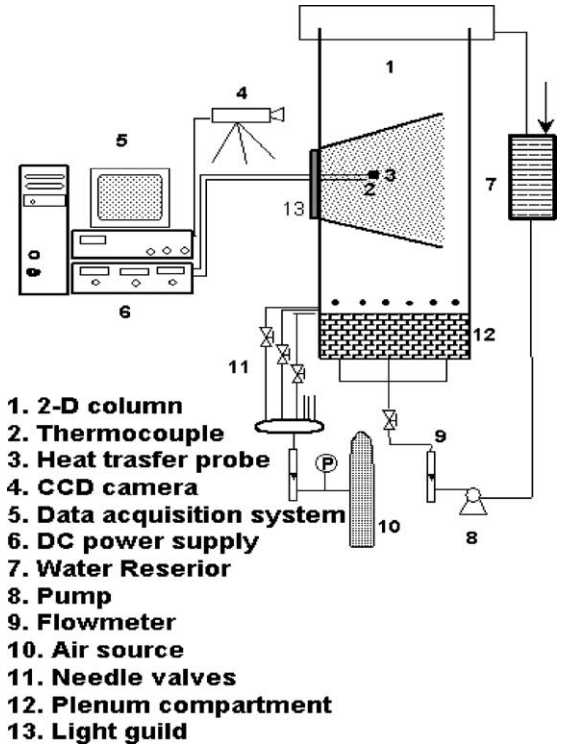

Fig. 1. Schematic diagram of the two-dimensional fluidized bed.

diameter 0.586 mm are used as solid phase. Sodium iodide solution is used as liquid phase to match the refractive index of the glass beads. The liquid solution is pumped into the bed through the bottom of the plenum compartment and is circulated back to the reservoir after discharged from the top of the column. A sieve situated at top of the column is applied to confine the solid particle from flowing out of the column. The level of the ebulated bed is maintained at 120 cm height in the study. Neutrally buoyant Pliolite particles of 500–600 μm are used as liquid seeding particles. The same diameter (0.586 mm) of glass beads painted with white color is used as solid tracer. Notice that the left hand side of the column is always investigated.

The heat transfer coefficient is measured by a heat transfer probe, as shown in Fig. 2, which consists six parts: T type thermocouple, micro-foil heat flux sensor, copper plate, foil heater, insulator, and supporting rod. The probe is placed vertically in between the acrylic sheets and can be moved to different locations in one run of experiment to measure the heat transfer. This probe with dimensions of 25 mm × 14 mm × 4 mm, uses a micro-foil heat-flux sensor, which is attached to a dc-powered heater. The local heat flux can be directly measured through the heating surface of the probe by detecting the temperature difference across a thermal barrier of a known thermal resistance. The sensor also gives the temperature of the heating surface. The bulk temperature is measured with a

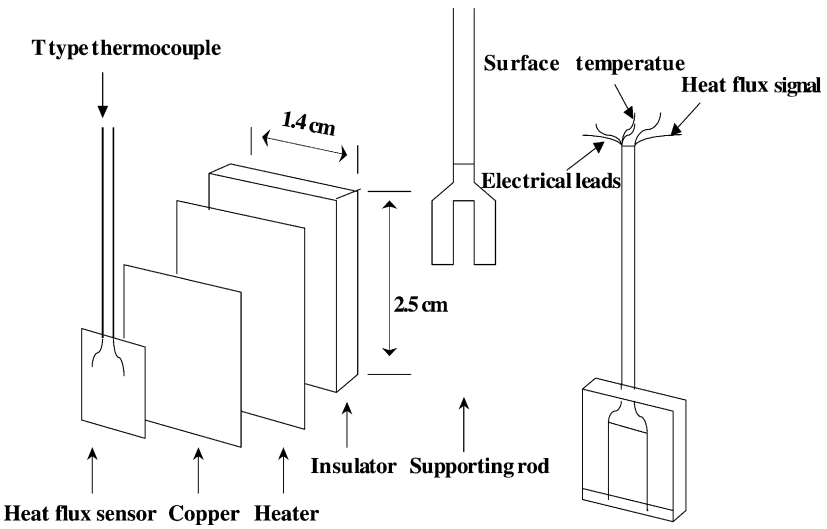

Fig. 2. The schematic and dimension of the heat transfer probe.

thermocouple, which is inserted horizontally into the bed. A data acquisition board interfaced with a PC computer digitizes the signals of the heat flux and the temperature difference between the probe surface and the bulk, at a sampling rate of 120 Hz for 40 s. With the heat flux and the temperature difference, the time-averaged heat transfer coefficient can be determined. In the text, all the gas velocities described refer to the superficial velocities unless otherwise stated.

Through the sidewall, a light sheet with 18 cm long is generated from a straight light guide. Connected with an optical fiber to the straight light guide, a 150 W halogen light source generator with a special filter lens provides a cold light to illuminate the flow field. Considering the resolution, the image field of view is limited to 16 cm × 19 cm from the left half of the column. The field of view is 30 cm above the liquid distributor. A high speed and high-resolution CCD camera is used to record the image of the flow field to the computer. A particle image analyzer (PIA) system developed by Chen and Chou [29] is applied to measure the bubble wake flow field in the 2D bubble columns. The technique of PIA discriminates between seeding particles and bubbles based on the size of the recorded image of the objects. There are five steps for the image processing, including image acquisition, image enhancement, particle identification and calculation of the centroids, discrimination of the particle images between the two phases, and matching of the particles in three consecutive video fields and calculation of the velocity of the identified triplets. The vectors obtained are located at the position of the centroid of the initial tracer particle in a triplet. A commercially available program, TECPLOT, is utilized for post-processing the PIA data. Through the utilization of advanced image acquisition and computer processing techniques, the PIA system is a non-intrusive technique, which provides quantitative results on a flow plane including instantaneous velocity distributions, velocity fluctuations, and other statistical flow information.

3. Results and discussion

3.1. Macroscopic flow structure

An example of the flow behaviors with increasing gas velocity is demonstrated in Fig. 3 as the dispersed bubbling regime and the coalesced bubbling regime. As $U_G < 1$ cm/s, the flow is in the dispersed bubbling regime characterized by a relatively uniform bubble size, as shown in Fig. 3(a). In this regime, the bubbles rise roughly rectilinear in the form of bubble streams. There is no coalescence or clustering of the bubbles in the individual bubble streams or with adjacent bubble streams. It is observed that the bubble size in the three-phase fluidized bed is significant larger than that in the bubble column. The liquid and solid phases are carried upward in the region of the bubble streams by the wake motion and fall downward between two adjacent bubble streams with continuous downward streams adjacent to the sidewalls.

When U_G is operated between 1 and 3 cm/s, the 4-region flow condition in the coalesced bubbling regime is encountered, as shown in Fig. 3(b). This flow structure comprises descending region, vortical region, fast bubble region, and central plume region. The fast bubble region, clustered together by bubbles at the bottom, moves in a wavelike manner, and thus the flow in the vicinity of this region is characterized macroscopically in terms of wave properties. Most of the solid particles are drifted upward by these two fast bubble streams and fall downward next to the sidewalls in the descending region. However, the coalescence is much less in the central plume region, and the bubble-bubble interactions are less significant.

Continuing increasing U_G over 3 cm/s, the flow regime transits to the 3-region flow condition, wherein two fast bubble flow regions merge together to form one central fast bubble region in the center of the column, as shown in Fig. 3(c). The gas flow in this regime is dominated by bubble coalescence and break-up. The wake effects drift the liquid–solid flow from the large bubbles rising in the center of the column. The vortical flow and descending flow regions are still observable. The flow condition is characterized by a gross circulation, in which the liquid–solid phase rises in the middle portion of the column and descends adjacent to the sidewalls. To illustrate the flow structure for each phase, Fig. 4 shows three consecutive original images, and liquid and solid streamline contours with $U_G = 3.34$ and $U_L = 10.5$ cm/s. It demonstrates that a large vortex progressively descends from the top to the bottom of the view. Some small bubbles and solid particles

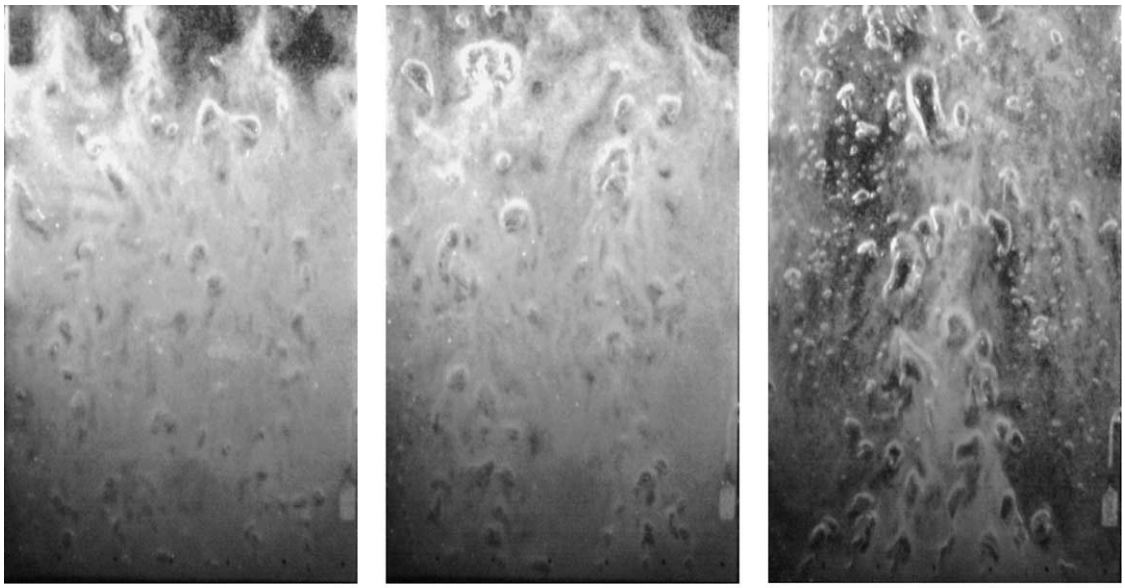

(a) dispersed bubbling regime (b) coalesced bubbling regime (4-region flow) (c) coalesced bubbling regime (3-region flow)

Fig. 3. Flow regimes in a two-dimensional three-phase fluidized bed.

are entrapped inside the vortical and descend flow regions. However, coupling with the inertial momentum and the gravity force, the entrapped solid particles descend faster and eventually separate from the vortex, as shown in Fig. 4(c). Furthermore, due to little influence by turbulent eddies, the streamline contour of solid phase is smoother than that of liquid. By averaging for a long period time, the radial distributions of the axial (v) and radial (u) velocities for gas, liquid and solid phases have been shown in Fig. 5. For all these three phases, the fast bubble stream region at the center of the column has the largest axial velocity. The upward velocity for each phase decreases sharply with radial direction and becomes zero at the location between 60 and 70% of the column half width. The result is similar to the 3D reported previously [28]. Additionally, because of the energy transfer, the gas phase has the largest upward axial velocity among these three phases. With the aid of gravity force, the solid phase has the largest downward velocity in vortical flow region. Due to the mass conservation, the radial velocity is close to zero for all phases.

3.2. Local heat transfer distribution

Fig. 6 shows the effects of solid holdup on the radial heat transfer distribution at three different flow regimes and $U_L = 10.5$ cm/s. For all three flow regimes, they show that the h significantly increases with solid holdup up to 8%, and then levels off or decreases with further increasing solid holdup. According to the consecutive film and surface renewal theory proposed by Kumar et al. [30], the initial increase on h at the low solid holdup can be attributed to the increase of contact frequency between solid particles and the probe. The increase of contact frequency consequently can enhance to destroy the liquid film on the surface of the probe and to renew a new liquid film, which lead to an increase of h. On the other hand, as pointed out by Barnea and Mizrahi [31] and Nigam and Schumpe [32], the high solid holdup can cause an increase in the pseduo-viscosity of the liquid–solid flow, which results in an increase in the bubble size and an reduced in the bubble terminal rise velocity. These large and slow bubbles generate less isotropic turbulence that reduces the effect of

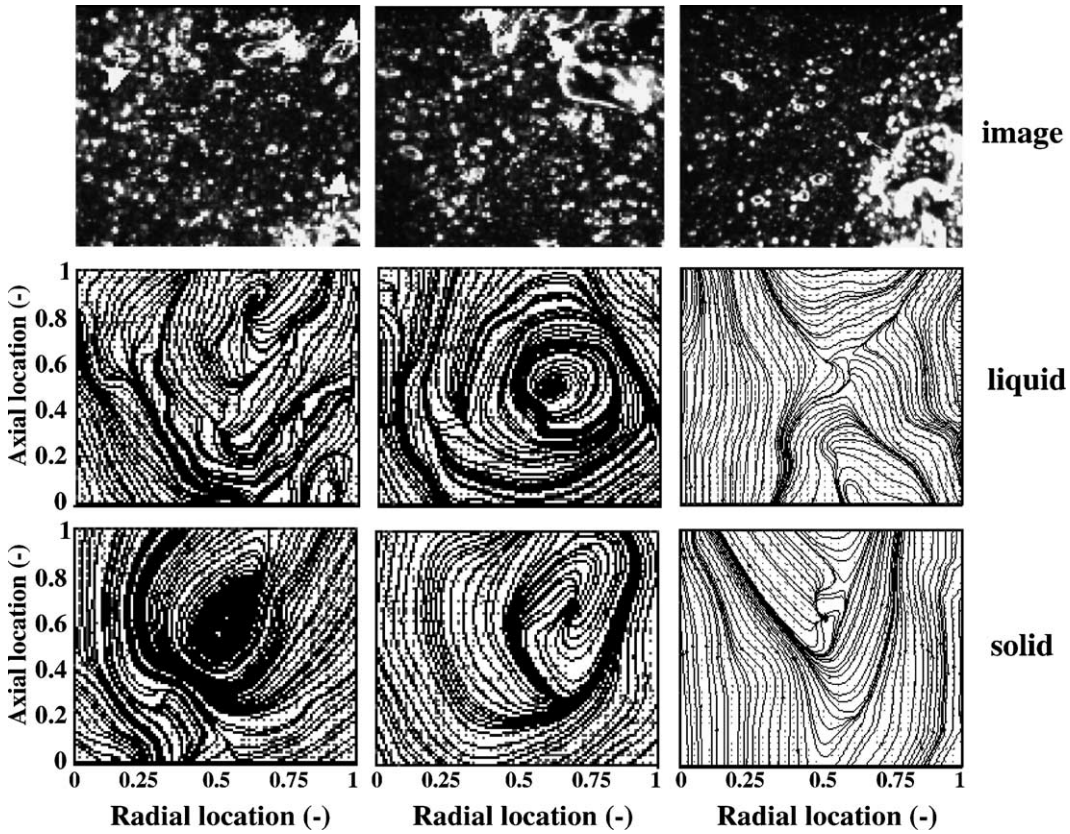

Fig. 4. Three consecutive original images, liquid and solid streamline contours at the in-bed location with: $U_G = 3.34$ and; $U_L = 10.5$ cm/s.

turbulent intensity on the heat transfer. Plus, the high pseduo-viscosity can diminish the turbulent eddies, dampen down the macroscopic structures, and thus lead to a decrease in heat transfer. The same result was reported by Li and Prakash [33] as well.

Fig. 6(a) shows a zigzag distribution on the radial h at $U_G = 0.2$ cm/s and $U_L = 10.5$ cm/s. The h induced by a strong turbulent intensity on the bubble streams is larger than that in between bubble streams and side-wall. Besides, it is noted that the contribution of the

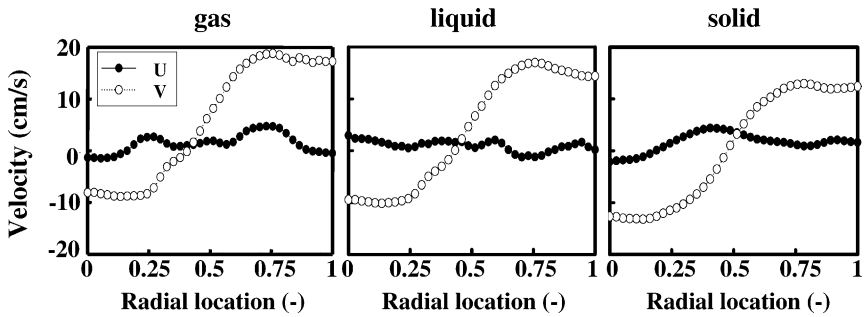

Fig. 5. Radial distributions of the axial (v) and radial (u) velocities for three phases with $U_G = 3.34$ and; $U_L = 10.5$ cm/s.

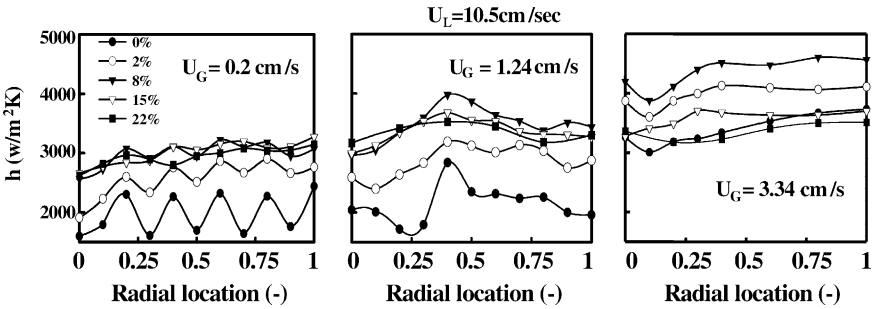

Fig. 6. Effects of solid holdup on the radial heat transfer distribution in three-phase fluidized beds at: (a) $U_G = 0.2$; (b) $U_g = 1.24$; (c) $U_g = 3.34$ and; $U_L = 10.5$ cm/s.

solid on the heat transfer is very significant. Increasing U_G to 1.24 cm/s, the flow is in the 4-region flow of the coalescence regime. Generally, the h in this regime is higher than that in the dispersed bubbling regime, as shown in Fig. 6(b). From this figure, the h reaches a maximum at the fast bubble stream region, wherein a high turbulent intensity is generated by the interaction of the drifted liquid and solid particles with the heat transfer probe. According to Mudde et al. [22] and Deckwer [4] studies, the fast bubble flow can generate the maximal normal Reynolds stresses (turbulent intensity), which are mainly responsible for the heat transfer. On the other hand, it shows that the vortical flow confines the liquid and small bubbles into a circulating cell, prevents interacting with its surrounding, and plays as a heat transfer barrier. This leads to the lowest value on the h in the vortical flow. The same result was also reported in Lin and Wang [23]. Nevertheless, the trapped bubbles and solid particles might weaken or even destroy the strength of the vortical flow. It is the reason why the heat transfer at the vortical flow region in the three-phase fluidized bed is not so drastically decreased as that in bubble columns. Most of the induced solid particles reaching to the top of column fall back to the descending flow region to form a downward liquid–solid flow. The downward liquid–solid flow promotes little effect on the h, and particularly becomes the worst heat transfer region at higher solid holdup. Further increasing gas velocity ($U_G = 3.34$ cm/s) to the 3-region flow, two fast bubble streams coalesce and form a large fast bubble flow region in the center of the bed. Fig. 6(c) illustrates that the distribution of the h in the radial direction at various solid holdups. For low solid holdups, the maximal h occurs at the fast bubble flow region and the minimal value is located in the vortical flow region. The same profile is also reported in the 3D literatures (e.g. Muroyama et al. [34]). Basically, the 3-region flow regime has the highest heat transfer rate in all three regimes due to the highly turbulent intensity generated by the large bubble wake. It is interesting to point out that the heat transfer in the descending region turns to a prominent increase because of the contribution of the strong Reynolds stresses induced by the descending liquid–solid flow with some entrapped bubbles.

3.3. Overall heat transfer (h_{ave})

By averaging the local radial heat transfer coefficient, the h_{ave} varies with gas velocity and solid holdup at $U_L = 10.5$ cm/s, as shown in Fig. 7(a). This figure shows that at a specific solid holdup the h_{ave} initially increases with gas velocity to a maximum, and then levels off with further increasing gas velocity. As mentioned in the previous, bubbles initially injected into the liquid–solid flow can increase the contact frequency between the solid particles and the probe, and intensify the turbulence of the liquid. However, the degree of turbulent intensity becomes poorer owing to the irregular distribution of bubbles at higher U_G and leads to the less isotropic turbulence that accordingly reduces the effect of turbulent intensity on the heat transfer. Additionally, this figure presents that the effect of U_G on the h_{ave} become less significant after 15% of solid holdup.

Fig. 7(b) demonstrates the h_{ave} varies with the liquid velocity and solid holdup at $U_G = 7.5$ cm/s. At low solid holdup (<15%), the h_{ave} gradually increases

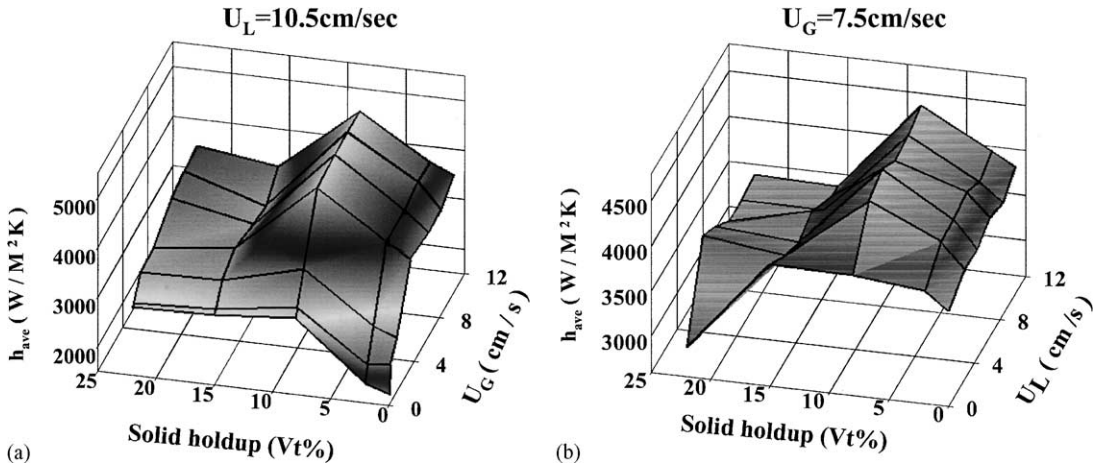

Fig. 7. Overall heat transfer coefficient varying with (a) gas velocity at $U_L = 10.5$ and; (b) liquid velocity at $U_G = 7.5$ cm/s at different solid holdups.

with the liquid velocity, and then keeps steadily with further increasing liquid velocity. The initial increase of the h_{ave} with U_L is as a result of the increase of turbulent intensity, vibrating the fluidized solid particles, and generating micro-eddies of the liquid elements inside the bed. However, the effect of liquid velocity on the h_{ave} is not so notable as that of gas velocity. Further increasing U_L, the solid holdup decreases and reduces the possibility of the erosion for overcoming the barrier next to the probe. The effects of the solid holdup on the h_{ave} are also illustrated in Fig. 7(a) and (b), and has been interpreted in the previous section.

4. Conclusions

The flow analysis and heat transfer measurement of three-phase fluidized beds based on the PIA technique and heat transfer probe, respectively, reveal that the heat transfer is influenced by the macroscopic hydrodynamic structures. With increasing gas velocity, the flow structures transit from dispersed bubble regime to coalesced bubble regime divided into the 4- and 3-region flows. In the dispersed bubbling regime, the h shows a zigzag distribution in radial the direction. In the bubble coalesced regime, the fast bubble region inducing bubble and solid particles has the maximal bubble size, liquid velocity, and heat transfer due to the strongest turbulent intensity. For the vortical flow region, the heat transfer in three-phase fluidized beds is larger than those in bubble column, because some small bubbles and solid particles entrapped can enhance the heat transfer by weakening the strength of vortex and increasing the surface contact frequency. Adding the solid particles can initially improve the collision frequency between the solid particles and heating object, which leads to the increase of heat transfer. However, over 8% of the solid holdup, the radial heat transfer becomes a lower and flatter distribution due to an increase in the pseduo-viscosity of the liquid–solid flow. In the beginning, the turbulent intensity induced by introducing the gas or liquid into the system is vital, and results to the increase on the h_{ave}. Further adding the gas and liquid, the effect on the h_{ave} turns out to be insignificant or even a negative.

Acknowledgements

The work was supported by the National Science Council grant 90-2214-E-194-008 in Republic of China.

References

[1] W.-D. Deckwer, Bubble Column Reactors, Wiley, New York, 1992.
[2] L.-S. Fan, Gas–Liquid–Solid Fluidization Engineering, Butterworths, Stoneham, MA, 1989.

[3] C.G.J. Baker, E.R. Armstrong, M.A. Bergougnou, Heat transfer in three-phase fluidized beds, Powder Technol. 21 (1978) 195.
[4] W.-D. Deckwer, On the mechanism of heat transfer in bubble column reactors, Chem. Eng. Sci. 35 (1980) 1341–1346.
[5] Y. Kato, K. Uchida, T. Kago, S. Morooka, Liquid holdup and heat transfer coefficient between bed and wall in liquid–solid and gas–liquid–solid fluidized beds, Powder Technol. 28 (1981) 173.
[6] Y. Kato, K. Uchida, T. Kago, S. Morooka, Heat transfer coefficient between an inserted vertical tube and a three-phase fluidized bed, Kagaku Kogaku Ronbunshu 10 (1984) 537.
[7] Y. Kang, I.S. Suh, S.D. Kim, Heat transfer characteristics of three-phase fluidized beds, Chem. Eng. Commun. 34 (1985) 1.
[8] S.C. Saxena, N.S. Rao, A.C. Saxena, Heat transfer from a cylindrical probe immersed in a three-phase slurry bubble column, Chem. Eng. J. 44 (1990) 144.
[9] S. Kumar, K. Kusakabe, L.-S. Fan, Heat transfer in three-phase fluidization and bubble columns with high gas holdups, AIChE J. 39 (1993) 1399.
[10] J.M. Kay, R.M. Nedderman, An Introduction to Fluid Mechanics and Heat Transfer, Cambridge University Press, Cambridge, 1974.
[11] D.A. Lewis, R.W. Field, A.M. Xavier, D. Edwards, Heat transfer in bubble columns, Trans. IchemE 60 (1982) 40.
[12] M. Magiliotou, Y.-M. Chen, L.-S. Fan, Bed-immersed object heat transfer in a three-phase fluidized bed, AIChE J. 34 (1988) 1043.
[13] S.D. Kim, A. Laurent, The state of knowledge on heat transfer in three-phase fluidized beds, Int. Chem. Eng. 31 (1991) 284.
[14] S.D. Kim, Y. Kang, Heat and mass transfer in three-phase fluidized bed reactor—an overview, Chem. Eng. Sci. 52 (1997) 3639.
[15] T.M. Chiu, E.N. Ziegler, Heat transfer in three-phase fluidized bed, AIChE J. 29 (1983) 677.
[16] K. Muroyama, M. Fukuma, A. Yasynishi, Wall-to-bed heat transfer in gas–liquid–solid fluidized beds, Can. J. Chem. Eng. 62 (1984) 199.
[17] K. Muroyama, L.-S. Fan, Fundamentals of gas–liquid–solid fluidization, AIChE J. 31 (1985) 1.
[18] N. Devanathan, D. Moslemian, M.P. Duduckovic, Flow mapping in bubble columns using CARPT, Chem. Eng. Sci. 45 (1990) 2285.
[19] T. Menzel, in: T. in der Weide, O. Staudacher, O. Wein, U. Onken (Eds.), Reynolds shear stress for modeling of bubble column reactors, Ind. Eng. Chem. Res. 29 (1990) 988.
[20] Z. Yang, U. Rustemeyer, R. Buchholz, U. Onken, Profile of liquid flow in bubble columns, Chem. Eng. Commun. 49 (1986) 51.
[21] T.-J. Lin, J. Reese, T. Hong, L.-S. Fan, Quantitative analysis and computation of two-dimensional bubble columns, AIChE J. 42 (1996) 301.
[22] R.F. Mudde, D.J. Lee, J. Reese, L.-S. Fan, Role of coherent structures on Reynolds stresses in a 2D bubble column, AIChE J. 43 (1997) 913.
[23] T.-J. Lin, S.-P. Wang, Effects of macroscopic hydrodynamics on heat transfer in bubble columns, Chem. Eng. Sci. 56 (2001) 1143.
[24] K. Tsuchiya, L.-S. Fan, Near-wake structure of a single gas bubble in a two-dimensional liquid–solid fluidized bed: vortex shedding and wake size variation, Chem. Eng. Sci. 43 (1988) 1167.
[25] T. Miyahara, T. Tsuchiya, L.-S. Fan, Wake properties of a single gas bubble in a three-dimensional liquid–solid fluidized bed, Int. J. Multiphase Flow 14 (1988) 749.
[26] R.-C. Chen, L.-S. Fan, Flow structure in a three-dimensional bubble column and three-phase fluidized bed, AIChE J. 40 (1994) 1093.
[27] H. Li, A. Prakash, Analysis of flow patterns in bubble and slurry bubble columns based on local heat transfer measurements, Chem. Eng. J. 86 (2002) 269.
[28] J.H. Hills, Radial non-uniformity of velocity and voidage in a bubble column, Trans. IchemE. 52 (1974) 1.
[29] R.-C. Chen, I.-S. Chou, Wake structure of a single bubble rising in a two-dimensional column, Exp. Therm. Fluid Sci. 17 (1998) 165.
[30] S. Kumar, K. Kusakabe, K. Raghunathan, L.-S. Fan, Mechanism of heat transfer in bubbly liquid–solid system: single bubble injection, AIChE J. 38 (1922) 733.
[31] E. Barnea, J. Mizrahi, A generalized approach fluid dynamics of particulate systems. Part 1. General correlation for fluidization and sedimentation in solid multiparticle systems, Chem. Eng. J. 5 (1973) 171.
[32] K.D.P. Nigam, A. Schumpe, Three-phase sparged reactor, Gordon and Breach, New York, 1996.
[33] H. Li, A. Prakash, Heat transfer and hydrodynamics in a three-phase slurry bubble column, Ind. Eng. Chem. Res. 36 (1997) 4688.
[34] K. Muroyama, M. Fukuma, A. Yasynishi, Wall-to-bed heat transfer in liquid–solid and gas–liquid–solid fluidized beds. Part II. Gas–liquid–solid fluidized beds, Can. J. Chem. Eng. 64 (1986) 409.